applied sciences

MDPI

Article

Optimum Design of High-Speed Single-Phase Flux Reversal Motor with Reduced Torque Ripple

Vladimir Dmitrievskii [1], Vladimir Prakht [1,*], Vadim Kazakbaev [1] and Dmitry Golovanov [2]

[1] Department of Electrical Engineering and Electric Technology Systems, Ural Federal University, 620002 Yekaterinburg, Russia; vladimir.dmitrievsky@urfu.ru (V.D.); vadim.kazakbaev@urfu.ru (V.K.)
[2] Department of Electrical Engineering, University of Nottingham, Nottingham NG7 2RD, UK; dmitry.golovanov@nottingham.ac.uk
* Correspondence: va.prakht@urfu.ru; Tel.: +7-343-375-45-07

Received: 18 August 2020; Accepted: 28 August 2020; Published: 31 August 2020

Featured Application: The presented results can be used in designing of single-phase high-speed electrical drives.

Abstract: Single-phase motors are used in low-power, cost-effective, variable-speed applications. As a replacement to traditional single-phase synchronous motors with magnets on the rotor, single-phase flux reversal motors (FRMs) with a rugged and reliable toothed rotor are considered for the high-speed applications. However, torque pulsations of single-phase motors are high. The aim of this work is to minimize the torque ripple and increase its minimum instantaneous value, as well as to reduce FRM losses. To solve this problem, an asymmetric rotor is used, and an objective function is proposed, which includes parameters characterizing the pulsations of the torque and the loss of FRM for two load conditions. To optimize the single-phase FRM and minimize the objective function, the Nelder–Mead method was applied. The optimization criterion was selected to maximize the efficiency, to reduce the torque ripple, and to the avoid the negative torque in a wide range of powers at the fan load (quadric dependence of torque on speed). Two operating loading modes are considered. After two stages of optimization, the peak-to-peak torque ripple in the FRM in the rated loading mode decreased by 1.7 times, and in the mode with reduced load by 2.7 times. In addition, in the FRM before optimization, the torque has sections with negative values, and in the FRM after optimization, the torque is positive over the entire period. Although losses in the rated mode increased by 4%, when underloaded, they decreased by 11%, which creates an additional advantage for applications that work most of the time with underload.

Keywords: electric machine design; flux reversal motor; high-speed motor; machines with magnets on the stator; mathematical modeling; optimal design; single-phase motor; special electric machines

1. Introduction

Single-phase motors are used in low-power, cost-effective, variable-speed applications. Various types of single-phase motors with magnets are known, such as a synchronous motor with magnets on the rotor surface [1–5] and motors with magnets on the stator [6–21]. The main advantage of single-phase motors compared to three-phase motors is the cheaper single-phase frequency converter. The main disadvantage of the single-phase machines is a low starting torque. Since the single-phase motors are cheap, they are used in low-cost variable speed drivers, such as fans [1,2], compressors [3], pumps [4], vacuum cleaners [5], and other household appliances and fluid machinery in which a high starting capability is not necessary.

The torque ripple of single-phase synchronous motors is much higher than that of three-phase motors. For instance, the torque ripple of the single-phase synchronous motor is 90% in [22] and 168% in [23], while that of the three-phase motor in [24] is 6.3%. The torque ripple of the brushed universal motor (AC commutator motor) is higher and can reach 300%, while the sign of the torque is the same during the entire electric period [25,26]. So, single-phase synchronous motors with lower torque ripple than of universal motor and with the torque of constant sign is an acceptable replacement for universal motors.

In high-speed applications, such as blowers, vacuum cleaners [5], and turbochargers [27,28], the rotors of these machines are designed with a retaining ring, which is mandatory in machines with permanent magnets on the rotor to withstand centrifugal stress and to ensure rotor durability [29]. However, the use of the retaining ring on the rotor increases the complexity and the cost of the rotor manufacturing. Furthermore, the use of the retaining ring leads to an increase in the equivalent air gap (the distance between the stator teeth and the permanent magnets), and to a decrease in the magnetic flux density in the air gap, the efficiency and the specific torque of the machine.

As a replacement to the single-phase synchronous machines with magnets on the rotor, motors with a rugged and reliable toothed rotor are considered for the high-speed applications [6–8]. One of these motors is a single-phase hybrid switched reluctance motor (HSRM) with magnets fixed on the stator, developed for a blender and described in [8].

In contrast to synchronous motors with magnets on the rotor, the HSRM has a simple toothed rotor without any magnets. The torque ripple of the single-phase HSRM [8] is 168%, and its torque is of constant sign throughout the entire electric period.

Regardless of the above-mentioned benefits of the HSRM over traditional single-phase motors, its drawback is that it is supplied by unipolar voltage pulses, while traditional synchronous motors are supplied by the bipolar AC voltage. As a result, to reach the same peak-to-peak value of the HSRM stator current, its root mean square (RMS) and maximum values need to be significantly higher than those of a similar single-phase traditional synchronous motor. Because of this, the cost and the size of the converter for the HSRM increase. The power losses in the converter and in the stator winding also increase.

Single-phase flux reversal machines (FRMs) have certain benefits over the HSRM and traditional synchronous motors. In contrast to traditional synchronous motors, an FRM has a simple and reliable toothed rotor similar to that of the HSRM. The use of permanent magnets mounted on the stator reduces its size and mass compared to the HSRM. Moreover, like traditional synchronous motors with magnets on the rotor, the FRM is supplied by bipolar voltage pulses. Current pulses of different signs in the FRM winding can occupy a larger part of the electrical period than in the HSRM. For this reason, the amplitude and RMS value of the FRM stator current decrease compared to the HSRM [9]. These make it possible to apply the switchers of a lower power in the frequency converter for the FRM. In addition, the DC-AC converter for an FRM has a lower power loss. Therefore, a smaller heat sink can be used, and the sizes of the converter can be smaller than in the case of the HSRM [9].

In recent years, many examples of three-phase FRMs have been discovered [10–13]. The three-phase motors, however, demand a more costly power converter and a more complex control. For this reason, the use of a single-phase FRM with the simple power converter and control configurations is preferred in the targeted applications.

Besides, all known three-phase FRMs [10–13] with an even number of the stator and rotor teeth have many poles and cannot be applied in high-speed applications due to high supply frequency, high losses in the steel and in the magnets.

Design of a single-phase FRM is not so often discussed in the literature. At present, only several various configurations of a single-phase FRM are known. The first basic configuration of a single-phase FRM was described in [14,15].

This motor design includes two teeth on the stator and three teeth on the rotor. Permanent magnets forming two poles on each of the stator teeth are installed on their surface. However, the single-phase

FRM configuration presented in [14] demonstrates the following drawbacks: (1) Only two-thirds of the internal surface of the stator are used; (2) the lifetime of the bearings decreases due to the radial force arisen from the asymmetry of the motor structure. These problems of the FRM [14] were resolved by another single-phase FRM described in [16,17].

In [17], a single-phase high-speed FRM was optimized for fan load in order to reduce losses (increase its efficiency). The torque pulsations in [17] were not included into the target function, therefore, their value is extremely large and equal to 335%. In addition, in the FRM [17], there is an interval at which the motor torque is negative.

In [21], a new design of a single-phase FRM with the asymmetric rotor was described to reduce torque pulsations. The new single-phase FRM with the asymmetric rotor was compared with the single-phase FRM with the symmetric rotor. In the rated mode, the calculated torque ripple for an asymmetric rotor FRM was reduced by 1.6 times compared to a symmetrical rotor of the FRM. However, in [21], the FRM was designed without using optimization methods; therefore, the characteristics of the FRM can be improved.

The aim of this work is to minimize the torque ripple and increase its minimum instantaneous value, as well as to reduce FRM losses. Few papers are dedicated to the optimization of single-phase high-speed machines. The optimization of the 1.5 kW, 40 krpm single-phase with the response surface method is considered in [30]. With the help of the optimization, the authors [30] tried to increase the efficiency, however, the torque oscillations were not considered. The 500 W, 100 krpm single-phase motor with magnets on the rotor is investigated in [31]. The authors decreased the cogging torque and the EMF (electromotive force) ripple, but the data on the torque ripple and the efficiency are not provided in [31]. In [32], the authors decreased the torque ripple, and achieved the positive torque throughout the electric period, but the efficiency was not investigated in [32].

In this work, to solve the optimization problem, an objective function is proposed, which includes parameters characterizing the pulsations of the torque and the loss of FRM for two load conditions. To optimize the single-phase FRM and minimize the function, the Nelder–Mead method was applied. After optimization, the torque ripple in the FRM in the nominal loading mode decreased by 1.7 times, and in the mode with reduced load by 2.7 times. In addition, after optimization, it was possible for the FRM to exclude sections with a negative value of the torque in the period. Although losses in the rated mode increased by 4%, when underloaded, they decreased by 11%, which creates an additional advantage for applications that work most of the time with underload.

2. Selection of Optimization Criteria for a Single-Phase Flux Reversal Motor

The goal of this optimization is to reduce the torque oscillations (TO) of a single-phase FRM. By TO, we mean the deviations of the instantaneous values of the torque from its average value. A traditional measure of this deviation is peak-to-peak value of torque ripple (PPTR). This criterion has proved itself well for multiphase machines, for which TO are poorly expressed and, as a result, negative values of the torque are absent on the entire period of the machine.

Single-phase motors [9,17,22,23,25,26] have significantly higher TO than three-phase motors [24,33,34], and as a result, instantaneous torque values can be negative. In order to increase the minimum value of the torque and, if possible, make it positive, in this paper, we introduce another criterion of TO—average to minimum torque difference (AMinTD), i.e., average torque value minus the minimum torque value in the given mode. Obviously, both the PPTR and AMinTD criteria are positive.

In this paper, we consider the optimization of a single-phase FRM operating in the fan load mode where the torque is proportional to the square of the speed. The considered speed range is from 80% to 100% of the rated speed of 18,000 rpm. The motor rated power is 754 W. Table 1 shows the characteristics of 2 considered modes of this range.

In general, the average efficiency over operation modes can be calculated as:

$$\eta = \frac{\sum\limits_i p_i P_{mech,i}}{\sum\limits_i p_i P_{A,i}}, \quad (1)$$

where p_i is the fraction of the time occupied with i-th mode; $P_{mech,i}$ and $P_{A,i}$.

Table 1. Motor operating points.

Mode Number	Rotational Speed, rpm	Torque, N·m	Mechanical Power, W
1	14,400 (80%)	0.256	386
2	18,000 (100%)	0.4	754

It is assumed that the motor most of the time operates with underload, and the fraction of the time occupied by the mode is approximately inversely proportional to real (active) power. On substituting, $p_i \sim 1/P_{A,i}$, (1) turns into arithmetical average. To optimize FRM, the objective function was minimized:

$$F = A \cdot B = < PPTR + 2 \cdot AMinTD > (1 - < Eff >), \quad (2)$$

where $A = < PPTR + 2 \cdot AMinTD >$, $B = 1 - < Eff >$ are optimization criteria, $< x > = (x_1 + x_2)/2$, means the arithmetic average of two modes, *Eff* is the motor efficiency.

Criterion A provides a reduction in the torque oscillations, criterion B provides a reduction in losses and an increase in motor efficiency. Both criteria are positive. The meaning of the multiplication is that a 1% decrease in A is considered as valuable as a 1% decrease in B. To optimize the single-phase FRM and minimize the target function (2), the Matlab implementation of the Nelder–Mead method (function "fminsearch") was used [35], since it does not require a gradient calculation and is applicable to noisy objective functions. The Nelder–Mead method is an unconstrained algorithm, and the region of the allowed parameters are not required. Only the objective function and the initial design must be provided. The noisiness of the objective functions (2) is due to rounding errors in the calculation based on the finite element method, as well as differences in the mesh for different calls to the objective function. Figure 1 shows parameters describing the design of the motor.

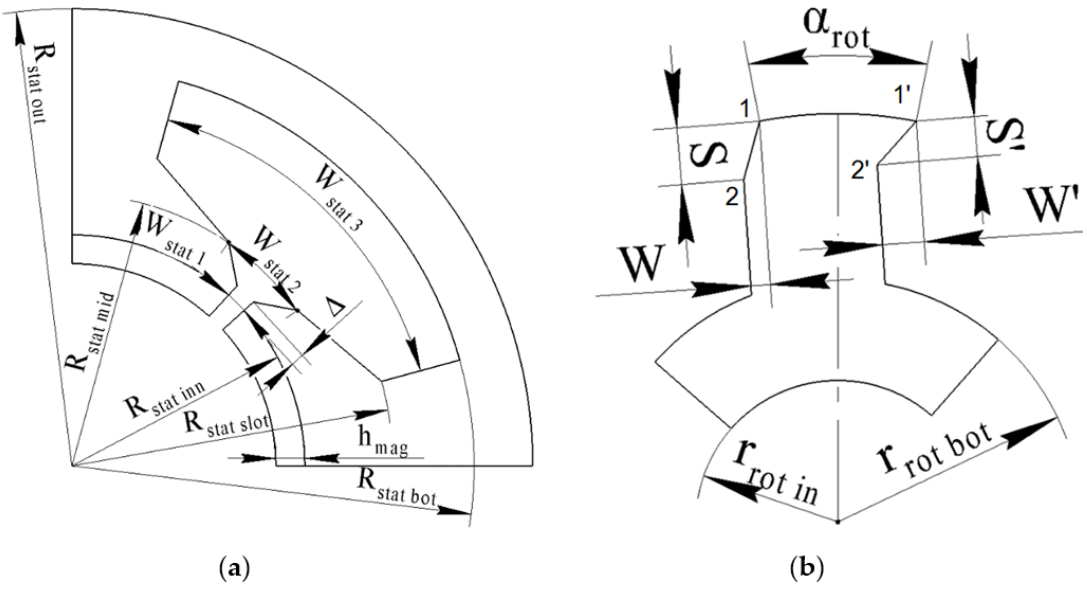

Figure 1. Motor design parameters: (**a**) stator; (**b**) rotor.

FRM is powered by a pulse-wise voltage of 320 V, 0 V, −320 V, 0 V. Moreover, the durations of the positive and negative pulses are equal. The periods of zero voltages are also equal to each other. In the simplest case, the middle of the voltage pulses falls on the rotor position in the middle between two positions: when the middle of the rotor arc facing the gap is above the middle of the slot opening, and when it is above the middle of the tooth (Figure 2a). Another optimization parameter is the shift of the voltage pulses forward along the rotor rotation relative to this simplest case (Figure 2b).

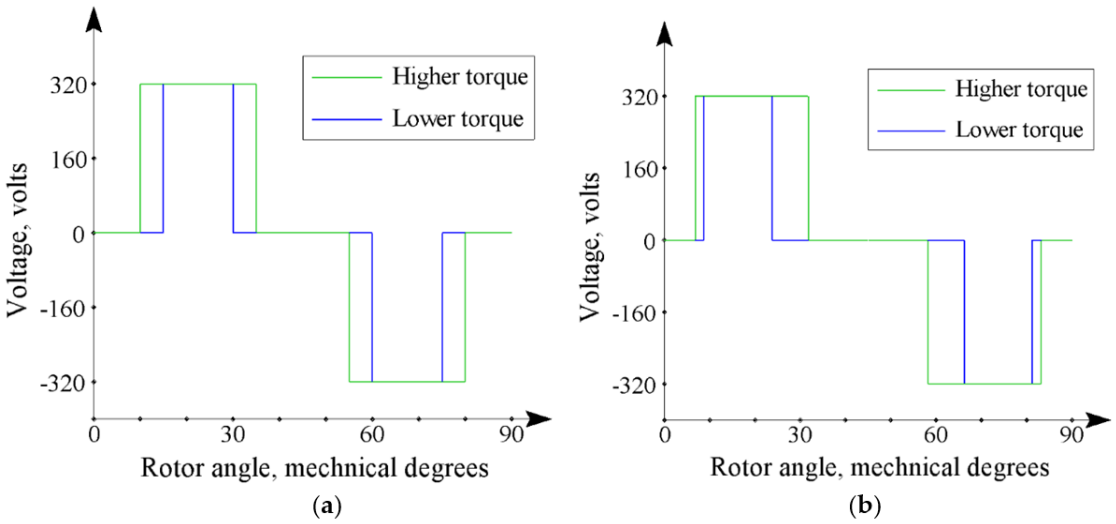

Figure 2. Supply voltage waveform: (**a**) basic case; (**b**) shifted pulses.

The mathematical model of FRM based on the finite element method is described in detail in [18,20]. First, the calculation is performed without taking into account losses. Therefore, for each timestep and the corresponding rotor position, the flux coupled to the winding is calculated by integrating the voltage. Then, for each position of the rotor and its corresponding flux, the magnetostatic problem is solved. Losses are taken into account in postprocessing afterwards. Table 2 shows the parameters that were not changed during optimization. Table 3 shows the parameters varied during the optimization.

Table 2. The FRM (flux reversal machine) parameters fixed during the optimization.

Parameter	Value
Supply voltage, V	320
Stator stack length L, mm	30
Stator outer radius, R_{outer}, mm	25.5
Stator slot width α_3, degrees	61.2
Stator slot width α_2, degrees	30.5
Δ, mm	0.007
Magnet thickness, mm	1.5
Air gap, mm	0.5
Remanence, T	1.2
s, mm	2
s', mm	3
$R_{rot\ bot}$, mm	7
R_{inner}, mm	3

For the stator and rotor cores, electrotechnical steel 35PN440 [36] was chosen, the thickness of the steel sheet is 0.35 mm. To reduce eddy current losses in magnets, each pole was divided into 8 segments over the cross section.

Table 3. The FRM parameters varied during the optimization. Additionally, $R_{stat,middle} = 0.5 \cdot (R_{stat,slot} + R_{stat,inner})$.

Parameter	Before	After
Number of turns per phase	80	91
$R_{stat,inner}$, mm	14	13.8
$R_{stat,slot}$, mm	18	17.4
$R_{stat,bottom}$, mm	22.5	22.463
$W_{stator1}$, degrees	8.1	15
α_{rot}, degrees	35.4	17.6
w/w_0	1	2.4119
w'/w_0	1	0.56176
Voltage shift, electrical radians	0.06	0.017426

3. Optimization Results

The design of the FRM before optimization is shown in Figure 3a. The motor in Figure 3a was designed without an optimization algorithm and is described in the article [9]. Figure 3b shows the optimized design.

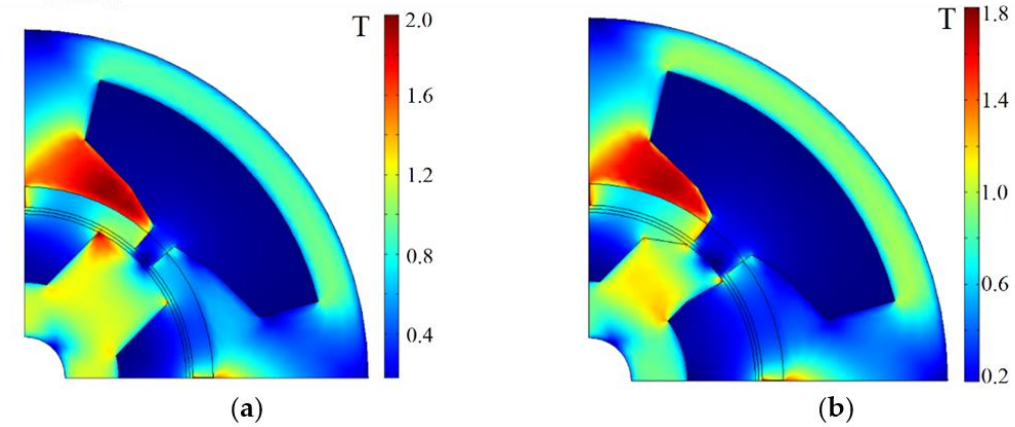

Figure 3. Motor design and simultaneous flux density field (T) in the FRM: (**a**) before optimization; (**b**) after.

Figure 4 shows the transient values of the torque depending on the rotor position for the modes specified in Table 1. In both modes, the torque waveform of the initial design takes negative values approximately in the middle of the first semi-period, while the optimization eliminates the negative values throughout the period. This is caused mainly by a nonuniform airgap formed by the line segment 1–2 (Figure 1b) in the direction of rotation. The transformation of the shape of the back side of the tooth with the line segment 1′–2′ (line segment between points 1′ and 2′ in Figure 1b) is not significant. Figures 5 and 6 show the transient values of the current and the voltage, depending on the rotor position for modes specified in Table 1. Forms of currents before and after optimization are almost identical.

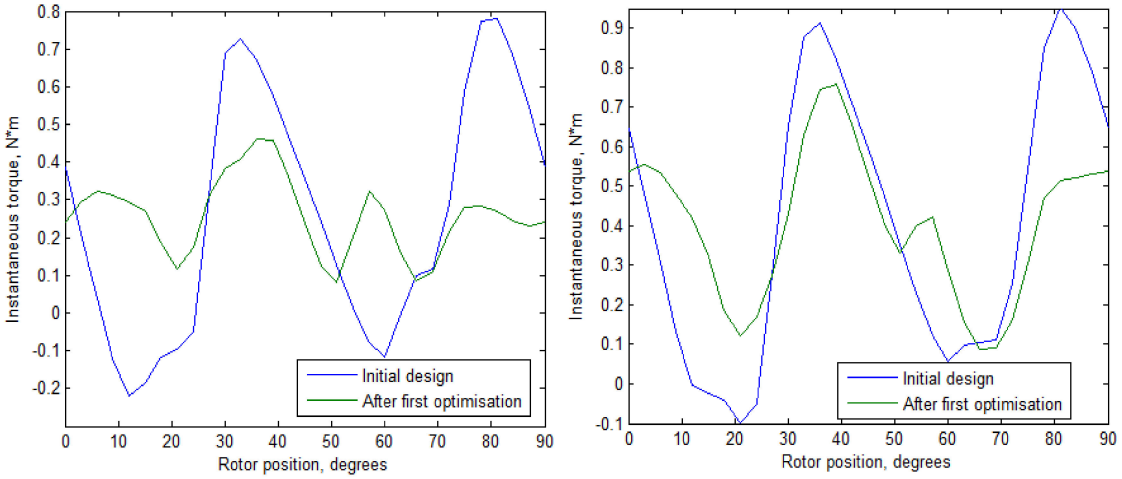

Figure 4. Torque dependencies on the rotor position before and after the optimization: (**a**) mode 1; (**b**) mode 2.

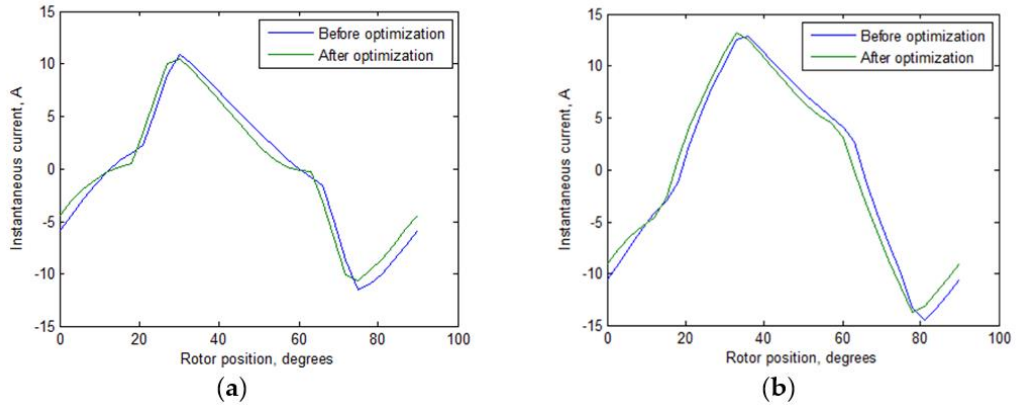

Figure 5. Current dependencies on the rotor position before and after the optimization: (**a**) mode 1; (**b**) mode 2.

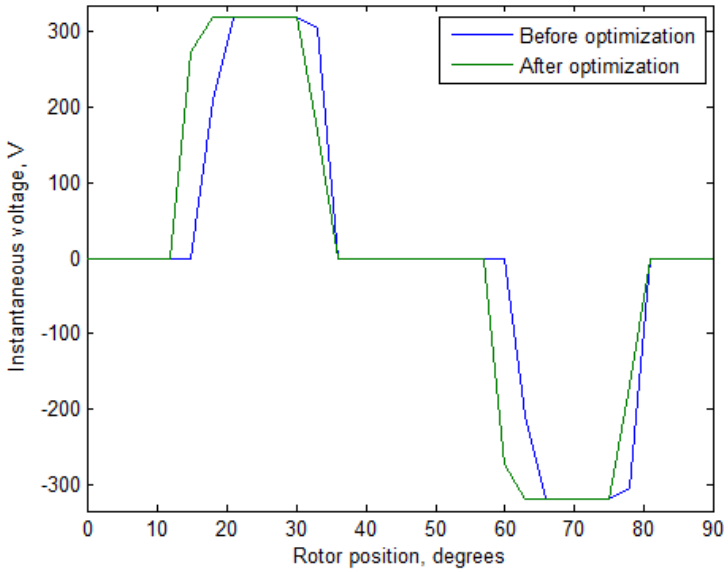

Figure 6. Voltage dependencies on the rotor position before and after optimization.

The change in the objective function (2) during optimization is shown in Figure 7. Changing the parameters included in the objective function (2) during the optimization is shown in Figures 8 and 9. Namely, Figure 8 shows the changes in motor efficiency during the optimization for modes specified in Table 1, and Figure 9 shows the change in the motor torque oscillations during the optimization. Figures show that the scattering of the parameters value becomes lower during the optimization that is the optimization converges. Table 4 shows the FRM characteristics before and after the optimization.

In Figure 10, the losses for both FRMs in two different modes are presented. Mechanical losses are estimated according to $5[W]\frac{n}{n_{rated}} + 10[W]\left(\frac{n}{n_{rated}}\right)^3$, where n—rotational speed n_{rated}—rated rotation speed of rotor 18,000 rpm.

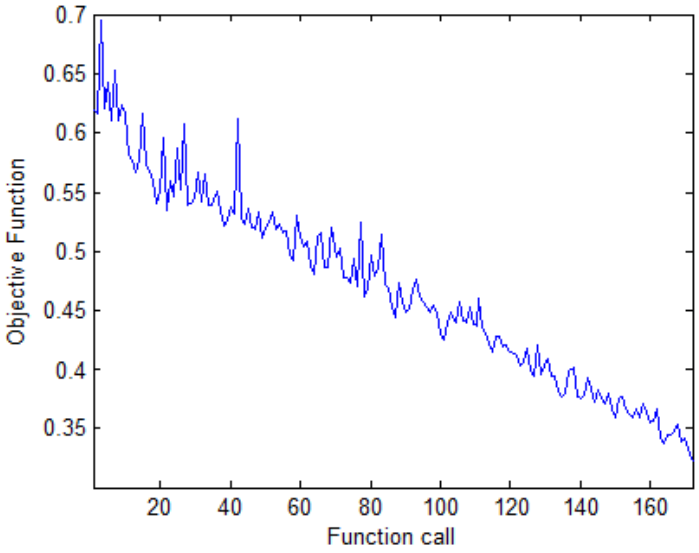

Figure 7. The objective function change during the optimization.

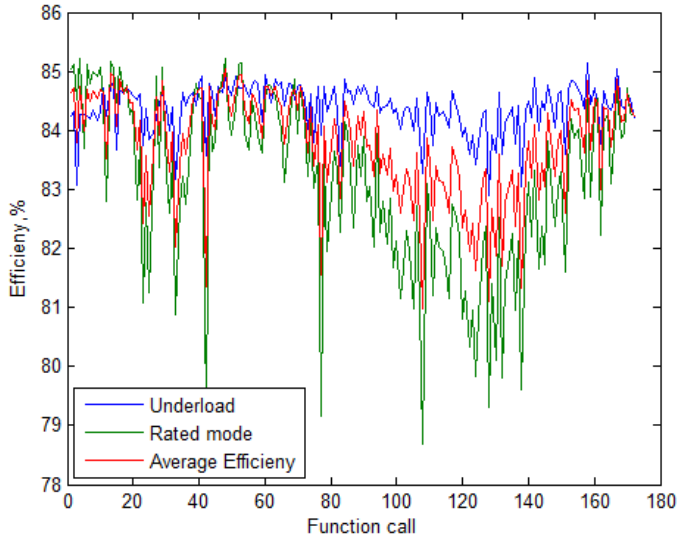

Figure 8. Change of the motor efficiency during the optimization.

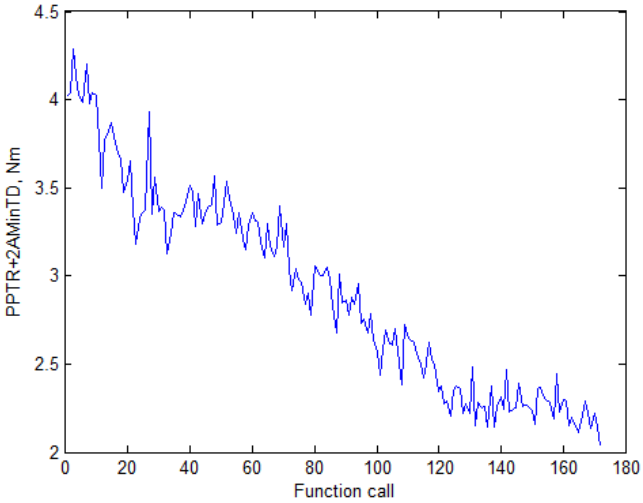

Figure 9. Change of the motor torque oscillations during the optimization.

Table 4. The FRM characteristics before and after the optimization.

Parameter	Before Optimization (Figure 3a)		After Optimization (Figure 3b)	
Speed, rpm	14,400	18,000	14,400	18,000
Current, A (RMS)	6.42	8.68	6.06	8.48
Efficiency, %	84.3	85.0	84.2	84.2
Total losses, W	70.5	130.1	70.8	138.1
Mechanical power, W	386	754	386	754
Electric power, W	447	869	448	877
Copper losses, W	44.1	80.5	48	94.2
Stator core losses, W	10.7	24.7	9.1	21.8
Rotor core losses, W	5.8	8.4	4.1	6.5
Magnet losses, W	0.8	1.4	0.4	0.8
Duty cycle	0.181	0.374	0.205	0.425
Minimal torque, N·m	−0.22	−0.1	0.081	0.089
AMinDT, N·m	0.476	0.5	0.175	0.311
PPTR, N·m	1	1.05	0.381	0.668
PPTR, % of the average value	391	263	149	167
Objective function, F	0.61884		0.32119	

It can be seen from Table 4 and Figure 4 that PPTR in the rated mode decreased by 1.6 times, and in the mode with reduced load by 2.6 times. In addition, for FRM before optimization, the torque has sections with negative values, and for FRM after optimization, the torque is positive over the entire period. The objective function F decreased by 1.9 times. However, FRM losses after optimization increased by 6% in the rated mode. Therefore, optimization (hereinafter referred to as the first optimization) was stopped and a second optimization was launched.

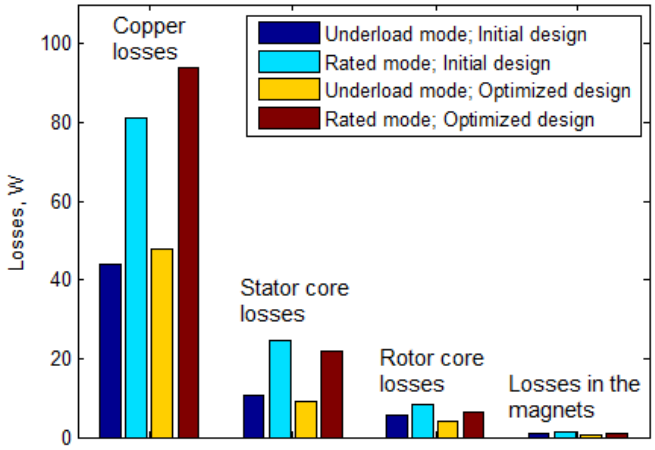

Figure 10. Losses for both FRMs in two modes.

4. The Second Optimization

As an initial approximation for the second optimization, the solution found after the first optimization was used. Such a restart of optimization solves the following problems. First, the simplex in the Nelder–Mead method can degenerate and the optimization process can slow down or stop before reaching the extremum. Secondly, during optimization, some parameters may change slowly. It can be expected that their change would be slow in the second optimization, therefore they can be excluded, which will accelerate the optimization process. Namely, the parameters $R_{stat,inner}$ and $R_{stat,bottom}$ were excluded. Thirdly, the optimization result is a compromise between the optimization criteria and one of the criteria may even deteriorate due to improvement in others, which can be negatively assessed by a person. To correct this situation, the objective function can be changed. Table 4 shows that despite a decrease in the torque oscillations (criterion A), criterion B increased (mean efficiency decreased) because of the increased copper losses. Therefore, the following optimization criterion was applied:

$$F_2 = A \cdot B^3 = <PPTR + 2 \cdot AMinTD> (1 - <Eff>)^3. \quad (3)$$

Fourth, when deleting some optimization parameters, it becomes possible to add new optimization parameters. The most significant losses are encountered in the winding (see Figure 10). Thus, we can assume that the change of the slot area significantly affects the efficiency. Therefore, the parameter $W_{stator\ 3}$ was added to the variable parameters. Figure 11 shows the FRM design after second optimization. Table 5 shows the FRM characteristics before and after the second optimization.

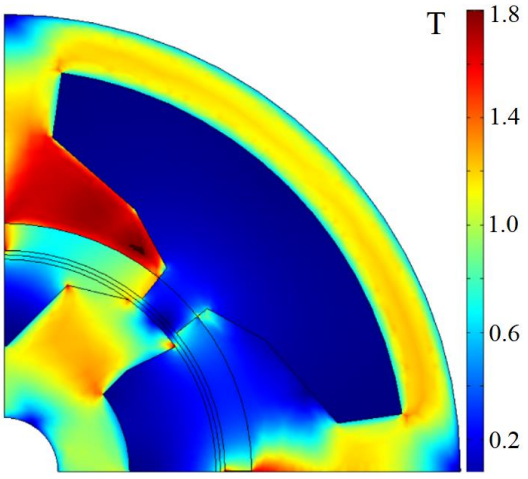

Figure 11. Motor design and simultaneous flux density field (T) in the FRM after second optimization.

Table 5. The FRM parameters varied during the second optimization.

Parameter	After First Optimization (Figure 3b)	After Second Optimization (Figure 11)
Number of turns per phase	91	115
$R_{stat\ slot}$, mm	17.4	18.8
$W_{stator\ 1}$, degrees	15	12.6
$W_{stator\ 3}$, degrees	61.2	72.9
$\alpha_{rot,}$ degrees	17.4	18
w/w_0	2.4119	2.63
w'/w_0	0.56176	0.471
Shift, electrical radians	0.017426	0.0146

The change in the objective function (2) during the second optimization is shown in Figure 12. The scattering and the changes in its value are almost stopped in the end of the second optimization, which means that the optimization process is almost over. The increase in the efficiency and the decrease in the torque oscillation are seen in Figures 13 and 14.

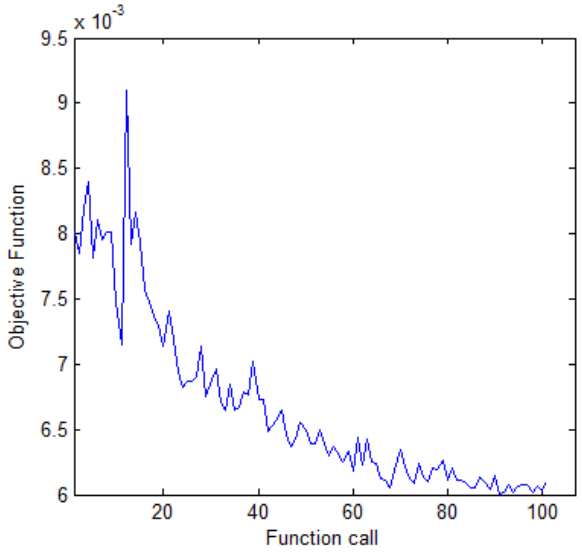

Figure 12. The objective function change during the second optimization.

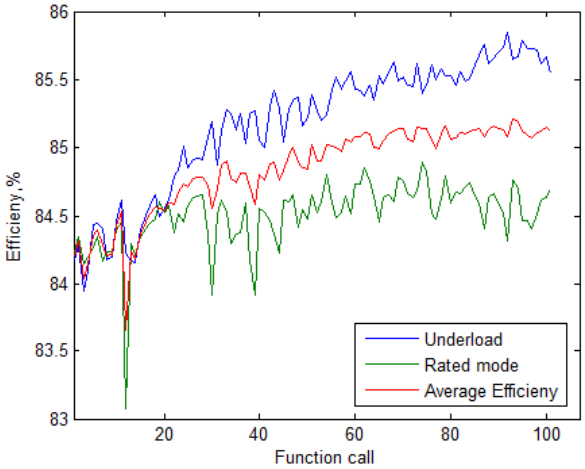

Figure 13. Change of the motor efficiency during the second optimization.

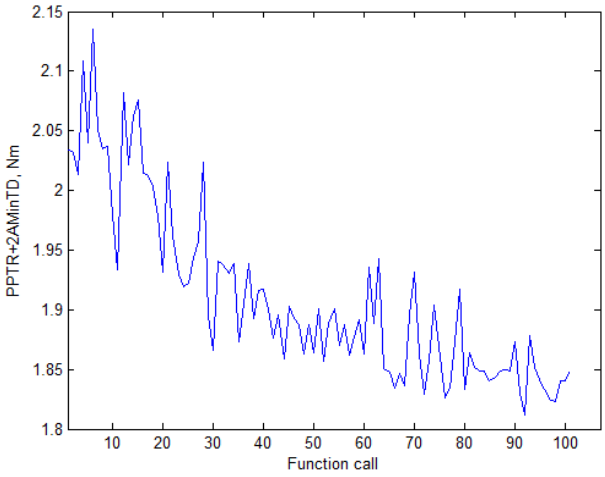

Figure 14. Change of the motor torque oscillations during the second optimization.

Figure 15 shows the decrease in PPTR and increase in the minimum instantaneous torque ripple. Changes in the current and voltage waveforms are shown in Figures 16 and 17.

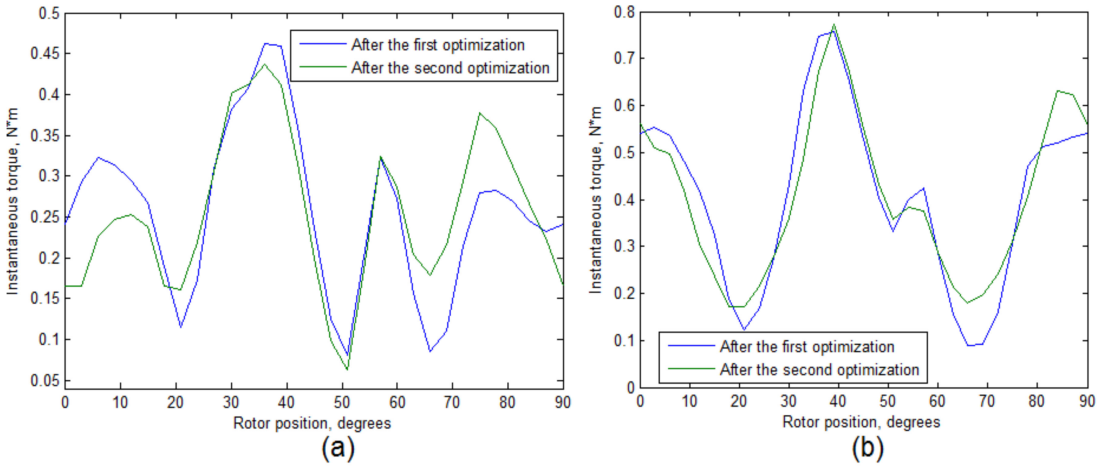

Figure 15. Torque dependencies on the rotor position before and after the second optimization: (**a**) mode 1; (**b**) mode 2.

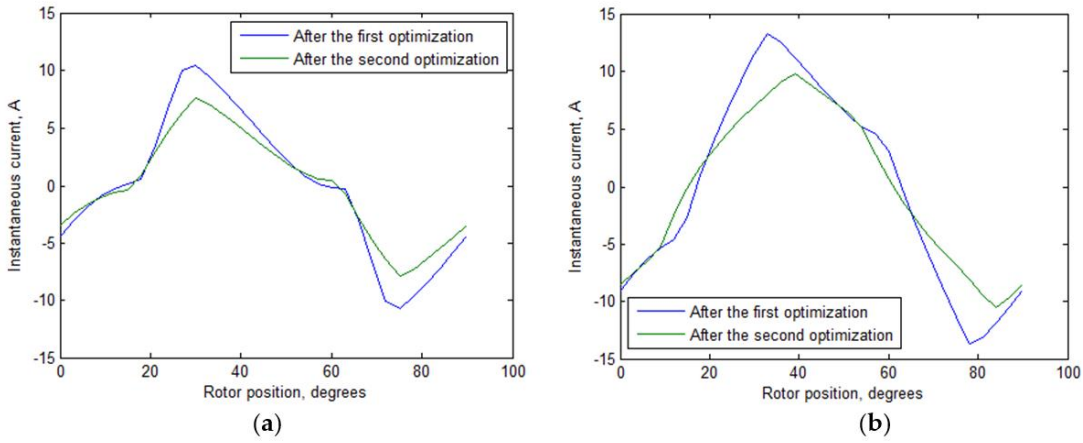

Figure 16. Current dependencies on the rotor position before and after the second optimization: (**a**) mode 1; (**b**) mode 2.

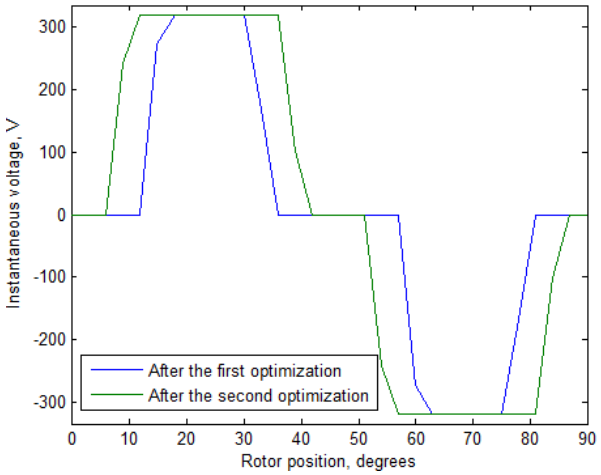

Figure 17. Voltage dependencies on the rotor position in the rated mode before and after the second optimization.

As it can be seen in Table 6 and Figure 18, the second optimization results are not only in a decrease in the parameter A (decrease in TO), but also in decrease in the parameter B: the efficiencies in both modes increases not only compared with the result of the first optimization, but even compared with the initial design. The increase in the efficiency is obtained due to the decrease in the copper losses.

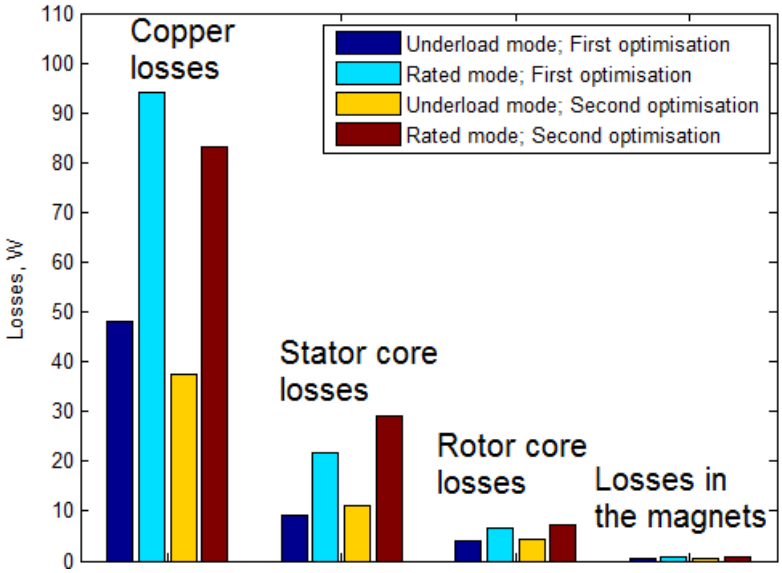

Figure 18. Losses for both FRMs in two modes.

As can be seen from Table 6, after changing the target function, it was possible to significantly increase the efficiency of the FRM by increasing the slot area and reducing the losses in the winding (Figure 10). In addition, the ripple of the torque in the rated mode decreased by 11%. The target function F_2 (3) decreased by 1.3 times after the second optimization.

Table 6. The FRM characteristics before and after the second optimization.

Parameter	After First Optimization (Figure 3b)		After Second Optimization (Figure 11)	
Speed, rpm	14,400	18,000	14,400	18,000
Current, A (RMS)	6.06	8.48	4.44	6.61
Efficiency, %	84.2	84.2	85.7	84.5
Total losses, W	70.8	138.1	62.7	135
Mechanical power, W	386	754	386	754
Electrical power, W	448	877	440	874
Copper losses, W	48	94.2	37.6	83.3
Stator core losses, W	9.1	21.8	11	29.1
Rotor core losses, W	4.1	6.5	4.5	7
Magnet losses, W	0.4	0.8	0.4	0.8
Duty cycle	0.205	0.425	0.297	0.672
Minimum torque, N·m	0.081	0.089	0.0623	0.171
AMinDT, N·m	0.175	0.311	0.193	0.229
PPTR, N·m	0.381	0.668	0.374	0.602
PPTR, % of the average value	149	167	146	150
Objective function F_2	0.00801		0.00601	

5. Conclusions

This paper describes the design optimization of a high-speed single-phase flux reversal motor with asymmetric rotor. The optimization criterion was selected to maximize the efficiency, to reduce the torque ripple, and to avoid the negative torque in a wide range of powers at the fan load (quadric dependence of torque on speed). Two operating modes are considered. A one-criterion Nelder–Mead method is used to optimize the motor design.

After two stages of optimization, the peak-to-peak torque ripple in the FRM in the rated loading mode decreased by 1.7 times, and in the mode with reduced load, by 2.7 times. In addition, in the FRM before optimization, the torque has sections with negative values, and in the FRM after optimization, the torque is positive over the entire electric period. Although losses in the rated mode increased by 4%, when underloaded, they decreased by 11%, which creates an additional advantage for applications that work most of the time with underload.

Author Contributions: Conceptual approach, V.P. and V.D.; data curation D.G. and V.K.; software V.D. and V.P.; calculations and modeling, V.P and V.D. and V.K.; writing of original draft, D.G., V.P., V.D. and V.K.; visualization, D.G., V.D. and V.K.; review and editing, D.G., V.P., V.D. and V.K. All authors have read and agreed to the published version of the manuscript.

Funding: The work was partially supported by the Ministry of Science and Higher Education of the Russian Federation (through the basic part of the government mandate, Project No. FEUZ-2020-0060).

Acknowledgments: The authors thank the editors and reviewers for careful reading, and constructive comments.

Conflicts of Interest: The authors declare no conflict of interest. The funders had no role in the design of the study; in the collection, analyses, or interpretation of data; in the writing of the manuscript, or in the decision to publish the results.

References

1. Fazil, M.; Rajagopal, K. Development of external rotor single-phase PM BLDC motor based drive for ceiling fan. In Proceedings of the 2010 Joint International Conference on Power Electronics, Drives and Energy Systems & 2010 Power India, New Delhi, India, 20–23 December 2010; Institute of Electrical and Electronics Engineers (IEEE): Piscataway Township, NJ, USA, 2010; pp. 1–4.
2. Hu, H.-J.; Cao, G.-Z.; Huang, S.-D.; Wu, C.; Peng, Y.-P. Drive circuit-based torque-ripple suppression method for single-phase BLDC fan motors to reduce acoustic noise. *IET Electr. Power Appl.* **2019**, *13*, 881–888. [CrossRef]
3. Lee, W.; Han, D.; Sarlioglu, B. Comparative Performance Analysis of Reference Voltage-Controlled Pulse Width Modulation for High-Speed Single-Phase Brushless DC Motor Drive. *IEEE Trans. Power Electron.* **2017**, *33*, 4560–4568. [CrossRef]
4. Ostovic, V. Performance comparison of U-Core and round-stator single-phase permanent-magnet motors for pump applications. *IEEE Trans. Ind. Appl.* **2002**, *38*, 476–482. [CrossRef]
5. Bentouati, S. Permanent magnet brushless dc motors for consumer products. In Proceedings of the 9th International Conference on Electrical Machines and Drives, Canterbury, UK, 1–3 September 1999; 1999; 1999, pp. 118–122. [CrossRef]
6. Török, V.; Loreth, K. The world's simplest motor for variable speed control? The Cyrano motor, a PM-biased SR-motor of high torque density. In Proceedings of the 1993 Fifth European Conf. Power Electronics and Applications, Brighton, UK, 13–16 September 1993; Available online: https://ieeexplore.ieee.org/document/264962 (accessed on 30 July 2020).
7. Török, V. Electric Motor with Combined Permanent and Electromagnets. U.S. Patent RE37027E, 2001. Available online: https://patents.google.com/patent/USRE37027 (accessed on 30 July 2020).
8. Jeong, K.; Ahn, J. Design and characteristics analysis of a novel single-phase hybrid SRM for blender application. *J. Electr. Eng. Technolo.* **2018**, *13*, 1996–2003. [CrossRef]
9. Prakht, V.; Dmitrievskii, V.; Kazakbaev, V.; Oshurbekov, S. Comparison of High-Speed Single-Phase Flux Reversal Motor and Hybrid Switched Reluctance Motor. In Proceedings of the 2019 20th International Symposium on Power Electronics (Ee), Novi Sad, Serbia, 23–26 October 2019; Institute of Electrical and Electronics Engineers (IEEE): Piscataway Township, NJ, USA, 2019; pp. 1–5.
10. Li, D.; Gao, Y.; Qu, R.; Li, J.; Huo, Y.; Ding, H. Design and Analysis of a Flux Reversal Machine With Evenly Distributed Permanent Magnets. *IEEE Trans. Ind. Appl.* **2018**, *54*, 172–183. [CrossRef]
11. Zhu, X.; Hua, W. An Improved Configuration for Cogging Torque Reduction in Flux-Reversal Permanent Magnet Machines. *IEEE Trans. Magn.* **2017**, *53*, 1–4. [CrossRef]
12. Vidhya, B.; Srinivas, K.N. Effect of stator permanent magnet thickness and rotor geometry modifications on the minimization of cogging torque of a flux reversal machine. *Turk. J. Electr. Eng. Comput. Sci.* **2017**, *25*, 4907–4922. [CrossRef]
13. Dmitrievskii, V.; Prakht, V. Gearless generator with magnets on the stator for wind turbine. *J. Physics Conf. Ser.* **2018**, *1102*, 012018. [CrossRef]
14. Deodhar, R.; Andersson, S.; Boldea, I.; Miller, T. The flux-reversal machine: A new brushless doubly-salient permanent-magnet machine. *IEEE Trans. Ind. Appl.* **1997**, *33*, 925–934. [CrossRef]
15. Deodhar, R.P.; Andersson, S.; Boldea, I.; Miller, T. The flux-reversal machine: A new brushless doubly-salient permanent-magnet machine. In Proceedings of the IAS '96. Conference Record of the 1996 IEEE Industry Applications Conference Thirty-First IAS Annual Meeting, San Diego, CA, USA, 6–10 October 1996; Institute of Electrical and Electronics Engineers (IEEE): Piscataway Township, NJ, USA, 2002; pp. 786–793.
16. Prakht, V.; Dmitrievskii, V.A.; Kazakbaev, V.; Oshurbekov, S. Comparative analysis of two high-speed single-phase electrical machines with permanent magnets on the stator. *Electr. Eng. Electromech.* **2020**, 20–25. [CrossRef]
17. Dmitrievskii, V.; Prakht, V.; Kazakbaev, V.; Sarapulov, S. Optimal Design of a High-Speed Single-Phase Flux Reversal Motor for Vacuum Cleaners. *Energies* **2018**, *11*, 3334. [CrossRef]
18. Dmitrievskii, V.; Prakht, V.; Pozdeev, A.; Klimarev, V.; Mikhalitsyn, A. Angular grinder with new flux reversal motor. In Proceedings of the 2015 18th International Conference on Electrical Machines and Systems (ICEMS), Pattaya, Thailand, 25–28 October 2015; Institute of Electrical and Electronics Engineers (IEEE): Piscataway Township, NJ, USA, 2015; pp. 1366–1371.

19. Kushwaha, D.; Dwivedi, A.; Reddy, R.; Srivastava, R.K. Study of 8/12 flux reversal machine as an alternator. In Proceedings of the 2014 21st International Conference on Telecommunications (ICT), Guwahati, India, 18–20 December 2014; Institute of Electrical and Electronics Engineers (IEEE): Piscataway Township, NJ, USA, 2015; pp. 1–4.
20. Prakht, V.; Dmitrievskii, V.; Kazakbaev, V.; Sarapulov, S. Steady-state model of a single-phase flux reversal motor. In Proceedings of the 2017 IEEE 58th International Scientific Conference on Power and Electrical Engineering of Riga Technical University (RTUCON, Riga, Latvia, 12–13 October 2017; Institute of Electrical and Electronics Engineers (IEEE): Piscataway Township, NJ, USA, 2017; pp. 1–5.
21. Prakht, V.; Dmitrievskii, V.; Kazakbaev, V. Novel Rotor Design for High-Speed Flux Reversal Motor. Energy Reports (ISSN: 2352-4847). In Proceedings of the 2020 7th International Conference on Power and Energy Systems Engineering (CPESE 2020), Fukuoka, Japan, 26–29 September 2020. Accepted for publication.
22. Bentouati, S.; Zhu, Z.Q.; Howe, D. Influence of design parameters on the starting torque of a single-phase PM brushless DC motor. *IEEE Trans. Magn.* **2000**, *36*, 3533–3536. [CrossRef]
23. Hwang, H.; Cho, J.; Hwang, S.-H.; Choi, J.Y.; Lee, C. Design of a Single-Phase BLDC Motor for a Cordless Vacuum Cleaner Considering the Efficiency of Airflow. *Energies* **2019**, *12*, 465. [CrossRef]
24. Fang, J.; Li, H.; Han, B. Torque Ripple Reduction in BLDC Torque Motor With Nonideal Back EMF. *IEEE Trans. Power Electron.* **2011**, *27*, 4630–4637. [CrossRef]
25. Niwa, Y.; Akiyama, Y. Propositions for the analysis of commutation phenomenon and the modeling of universal motors based on introducing the state function method into FEM electromagnetic field analysis. In Proceedings of the 2009 IEEE Energy Conversion Congress and Exposition, San Jose, CA, USA, 20–24 September 2009 ; 2009; pp. 226–233. [CrossRef]
26. Lin, D.; Zhou, P.; Stanton, S. An analytical model and parameter computation for universal motors. In Proceedings of the 2011 IEEE International Electric Machines & Drives Conference (IEMDC), Niagara Falls, ON, Canada, 15–18 May 2011; Institute of Electrical and Electronics Engineers (IEEE): Niagara Falls, ON, Canada, 2011; pp. 119–124.
27. Lee, W.; Kim, J.H.; Choi, W.; Sarlioglu, B. Torque Ripple Minimization Control Technique of High-Speed Single-Phase Brushless DC Motor for Electric Turbocharger. *IEEE Trans. Veh. Technol.* **2018**, *67*, 10357–10365. [CrossRef]
28. Zhu, Z.; Chen, Y.; Li, Y.; Howe, D.; Gliemann, J. Dynamic modelling of a high-speed single-phase PM brushless DC drive. In Proceedings of the 3rd IET International Conference on Power Electronics, Machines and Drives (PEMD 2006), Dublin, Ireland, 4–6 April 2006; Institution of Engineering and Technology (IET): Dublin, Ireland, 2006; pp. 484–488.
29. Cupertino, F.; Cupertino, F.; Monopoli, V.G.; Cascella, G.L. Design Procedure for High-Speed PM Motors Aided by Optimization Algorithms. *Machines* **2018**, *6*, 5. [CrossRef]
30. Choi, J.-H.; Koo, D.-H.; Kim, S.; Kim, Y.-H.; Ahn, J.; Cho, C.-H.; Lee, J. Approximate optimization for maximum efficiency of high speed single phase switched reluctance motor using response surface modelling. *Int. J. Appl. Electromagn. Mech.* **2008**, *28*, 227–235. [CrossRef]
31. Xia, S.; Wang, S.; Bi, D. Control Performance of High-Speed Single-Phase Brushless DC Motors. In Proceedings of the 2019 22nd International Conference on Electrical Machines and Systems (ICEMS), Harbin, China, 11–14 August 2019; Institute of Electrical and Electronics Engineers (IEEE): Harbin, China, 2019; pp. 1–6.
32. Chen, Y.; Chen, S.; Zhu, Z.; Howe, D.; Ye, Y. Starting Torque of Single-Phase Flux-Switching Permanent Magnet Motors. *IEEE Trans. Magn.* **2006**, *42*, 3416–3418. [CrossRef]
33. Dmitrievskii, V.; Prakht, V.; Kazakbaev, V. IE5 Energy-Efficiency Class Synchronous Reluctance Motor With Fractional Slot Winding. *IEEE Trans. Ind. Appl.* **2019**, *55*, 4676–4684. [CrossRef]
34. Cupertino, F.; Pellegrino, G.; Gerada, C. Design of synchronous reluctance machines with multi-objective optimization algorithms. In Proceedings of the 2013 IEEE Energy Conversion Congress and Exposition, Denver, CO, USA, 15–19 September 2013; 2013; 50, pp. 1858–1865. [CrossRef]

35. Audet, C.; Tribes, C. Mesh-based Nelder-Mead algorithm for inequality constrained optimization. *Comput. Optim. Appl.* **2018**, *71*, 331–352. [CrossRef]
36. Non-oriented Electrical steel, Posco, product catalogue. 2019. Available online: http://www.steel-n.com/e-sales/pdf/en/e_electrical_pdf_NO_2020.pdf (accessed on 30 July 2020).